PAPER • OPEN ACCESS

# Neon seeding effects on two high-performance baseline plasmas on the Joint European Torus

To cite this article: S. Gabriellini *et al* 2023 *Nucl. Fusion* **63** 086025

OPEN ACCESS
IOP Publishing | International Atomic Energy Agency
Nuclear Fusion
Nucl. Fusion **63** (2023) 086025 (10pp)
https://doi.org/10.1088/1741-4326/ace2d7

# Neon seeding effects on two high-performance baseline plasmas on the Joint European Torus

**S. Gabriellini[1,*], L. Garzotti[2], V.K. Zotta[1], C. Bourdelle[3], F.J. Casson[2], J. Citrin[4,5], D. Frigione[6], R. Gatto[1], C. Giroud[2], F. Koechl[2], P. Lomas[2], M. Marin[4], S. Menmuir[2], G. Pucella[7], F. Rimini[2], D. van Eester[8] and JET Contributors[a]**

[1] Department of Astronautical, Electrical and Energy Engineering, Sapienza University of Rome, Via Eudossiana 18, Rome, 00184, Italy
[2] United Kingdom Atomic Energy Authority, Culham Science Centre, Abingdon, Oxfordshire, OX14 3DB, United Kingdom of Great Britain and Northern Ireland
[3] CEA, IRFM, F-13108 Saint Paul Lez Durance, France
[4] DIFFER—Dutch Institute for Fundamental Energy Research, Eindhoven, Netherlands
[5] Science and Technology of Nuclear Fusion Group, Eindhoven University of Technology, Eindhoven, Netherlands
[6] University of Rome Tor Vergata, Via del Politecnico 1, Rome, 00133, Italy
[7] ENEA C. R. Frascati, Frascati, Italy
[8] Laboratory for Plasma Physics, LPP-ERK/KMS, Bruxelles Belgium

E-mail: stefano.gabriellini@uniroma1.it

Received 3 April 2023, revised 7 June 2023
Accepted for publication 29 June 2023
Published 11 July 2023

**Abstract**

We present the JETTO-QuaLiKiz-SANCO fully predictive modelling of two JET-ILW high-performance baseline plasmas, a Ne seeded shot and an equivalent unseeded one. The motivation of the work lies in the experimental observation of a slightly higher confinement and performance of the Ne seeded shot with respect to the unseeded one, despite sharing the same main plasma parameters and heating powers. Moreover, the neon seeded shot shows a lower pedestal electron density and a higher core ion temperature with respect to the unseeded one. Integrated modelling is performed in order to understand if the cause of the improved confinement has to be ascribed to the improved pedestal parameters with neon seeding or if an impurity-induced turbulence stabilization is at play. The QuaLiKiz transport model is used for predicting the electron density, electron and ion temperatures and rotation in the core up to the pedestal top, while the pedestal is empirically modelled to reproduce the experimental kinetic profiles. The thermal diffusivities of the two shots, computed by QuaLiKiz, are compared, as well as the turbulence spectra, suggesting that the reduced transport found in the neon seeded shot is due in part to the stabilization of ion temperature gradient and electron temperature gradient modes. Further modelling is performed in order to disentangle the neon seeding effects, which are a direct effect on the turbulence stabilization and an indirect effect on the pedestal parameters. The results suggest that the improved performance with neon is due to a combination of turbulence stabilization and improved pedestal parameters.

[a] See Mailloux *et al* 2022 (https://doi.org/10.1088/1741-4326/ac47b4) for JET Contributors.
[*] Author to whom any correspondence should be addressed.

Keywords: nuclear fusion, magnetic confinement, tokamak, JET, impurity seeding, turbulence, modelling

(Some figures may appear in colour only in the online journal)

## 1. Introduction

The optimization of the confinement of energy and particles in magnetically confined plasmas is crucial for reaching high fusion performances. In order to achieve thermonuclear conditions, particles need to be confined inside the plasma for a sufficient amount of time for fusion reactions to occur [1]. However, transport processes cause particles and energy to escape from the plasma, leading to a degradation of the confinement.

The transport observed in tokamak experiments is much higher than the neoclassical transport predicted by theory, and it is governed by micro-scale turbulences, which are mainly driven by gradients of temperature or density. One technique that can lead to turbulence stabilization is the controlled injection of impurities [2, 3]. In fact, it has been demonstrated on different tokamaks that the seeding of impurities (mainly neon) into the plasma can lead to a higher confinement with respect to equivalent unseeded pulses [2–6]. In addition to this, the injection of low-to-mid Z impurities (e.g. N or Ne) is primarily useful for mitigating heat fluxes to the divertor by reaching detached or semi-detached conditions [4]. However, (semi-)detached plasmas in JET do not achieve extremely high performance in terms of fusion power. The aim of the experiment modelled here was to investigate whether Ne seeding in plasmas already optimized for maximum performance (i.e. low fueling, pellet edge localized mode (ELM) pacing, fully attached divertor) would result in a further enhancement of the performance.

In this paper we investigate the effects of neon seeding on transport and confinement by modelling two JET high-performance baseline pulses, a Ne-seeded pulse and an equivalent unseeded one, which share the same main plasma parameters and auxiliary heating powers. However, the Ne seeded pulse shows a higher neutron rate (+17.9%) and energy confinement time (+14.0%) with respect to the unseeded one. Comparing the experimental kinetic profiles, one finds that the main differences between the two pulses are the lower electron density pedestal and the higher core ion temperature of the Ne seeded shot. The latter is probably due to the higher ion temperature pedestal, which propagates into the core because of the stiffness of the profiles. The improved pedestal achieved in the neon seeded case allows for a deeper penetration of the neutral beam injection (NBI) due to the lower electron density and, at the same time, for a higher core ion temperature due to the higher ion temperature pedestal. Both of these differences in the pedestal region are contributing to the performance and to the confinement of the Ne seeded discharge. Therefore, the goal of this study is to understand whether the higher confinement of the Ne seeded shot has to be ascribed solely to the pedestal improvement with neon or if a modification of the core transport is at play.

The integrated modelling of the discharges was carried out with the JINTRAC [7] suite of codes and the QuaLiKiz [8, 9] first-principle transport model.

The paper is organized as follows: in section 2 we describe the experimental discharges, in section 3 we present the modelling settings and the agreement between experiments and simulations, in section 4 we discuss the effects of neon on transport and confinement and in section 5 we summarize the main conclusions of the study.

## 2. Experimental discharges

The shots analyzed in this work, JPN 96994 (Ne seeded) and JPN 96730 (unseeded), are two baseline D–D ELMy H-modes at 3 MA/2.8 T, with $\beta_N \approx 2.2$ and $q_{95} \approx 3.2$. The baseline is one of the plasma scenarios developed at the Joint European Torus (JET) for achieving high fusion power with a steady performance, characterized by a high plasma current and magnetic field and a moderate normalized $\beta$, with a relaxed current profile [10]. The neon seeded shot was developed to assess the impact of impurity seeding on fusion performance and was able to reach the highest neutron rate over 5 s among the DD baseline shots, as reported in [12]. However, it differs from other JET neon seeded scenarios, such as the one described in [4], in the fact that JPN 96 994 has a lower neon seeding, lower recycling, lower gas puff, lower edge collisionality and a higher performance.

In the following section the parameters that will be listed are averaged in the modelled time interval (from 10.02 to 12.02 s), unless stated otherwise.

A comparison between the main experimental time traces is presented in figure 1, where we show the NBI and ion cyclotron resonance heating (ICRH) heating powers and plasma bulk radiated power, plasma diamagnetic energy content and normalized $\beta$, $Z_{\text{eff}}$, total gas fueling rate and neon fueling rate, core and edge electron density, core electron temperature, core ion temperature, Be II emission (indicative of the ELMs activity) and neutron yield. Details on the diagnostics are given in the figure caption.

As we can see from the top box of the figure, the two shots have a similar heating power and a comparable plasma radiation. The neon seeded shot has a heating power of 31 MW, 28 MW from NBI and 3.3 MW from ICRH in H minority scheme, while the unseeded shot has a slightly higher power of 33 MW, 29 MW from NBI and 4.1 MW from ICRH in H minority scheme. The radiation fraction, defined here as $f_{\text{rad}} = P_{\text{rad}}/P_{\text{in}}$ (where $P_{\text{rad}}$ is the bulk radiated power and $P_{\text{in}}$ is the power injected into the plasma), is very close between the pulses and equal to $f_{\text{rad}} \approx 0.30$.

The plasma diamagnetic energy and the normalized $\beta$ are also very similar and equal to $W_{\text{dia}} \approx 9$ MJ and $\beta_N \approx 2.2$.

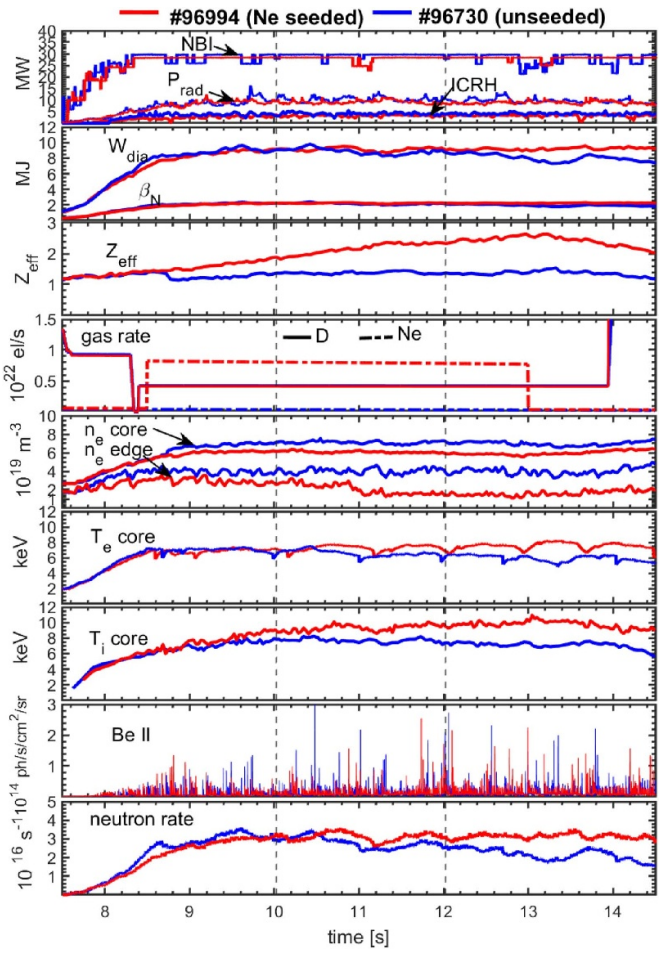


**Figure 1.** Experimental time traces comparison between JET shot #96994 in red (Ne seeded) and #96730 in blue (unseeded). From top to bottom are shown: NBI and ICRH heating powers and bulk radiated power, plasma diamagnetic energy and $\beta_N$ (from a pressure constrained EFIT [11] equilibrium reconstruction), $Z_{\text{eff}}$ (from visible spectroscopy and Bremsstrahlung measurements along a horizontal line of sight), total (solid line) and neon (dashed line) gas rates, core and edge line averaged electron density (from JET far infrared interferometer with line of sights at a major radius of 3.03 m and 3.73 m respectively), core electron temperature (from electron cyclotron emission radiometer at a major radius of 3.1 m), core ion temperature (from high resolution x-ray crystal spectrometer at $\Psi_N = 0.19$), Be II emission (from visible spectroscopy, showing ELMs behavior), neutron rate.

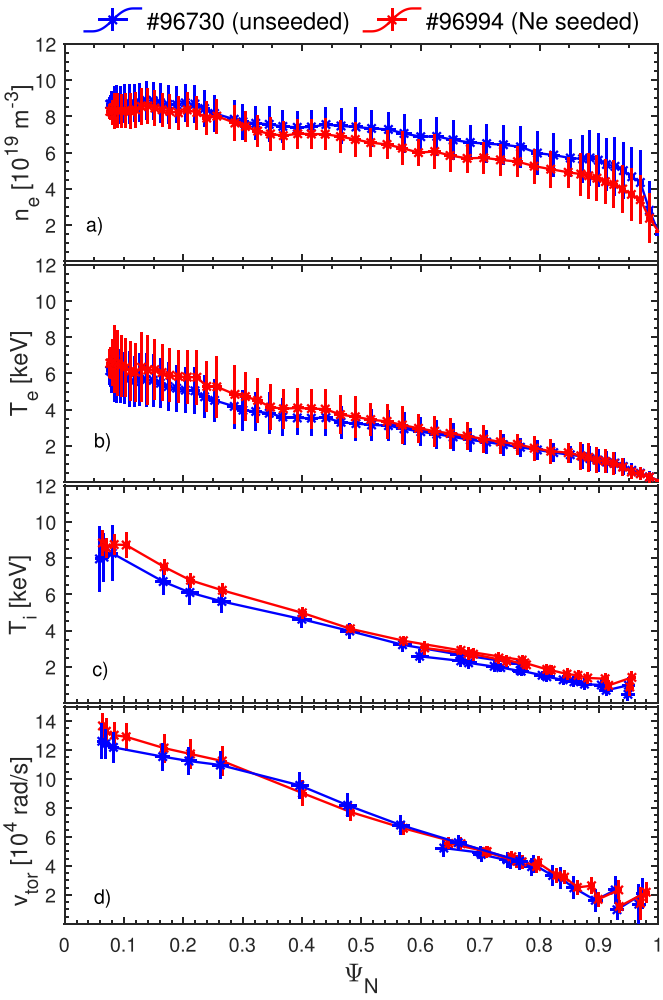


**Figure 2.** Comparison between experimental profiles of electron density (*a*), electron temperature (*b*), ion temperature (*c*) and toroidal rotation (*d*) between 10.02 and 12.02 s. The electron density and temperature profiles are taken from high resolution Thomson scattering measurements (HRTS), while the ion temperature and toroidal rotation profiles are taken from beam charge exchange spectroscopy (CX). The vertical error bars combine the RMS over the time interval considered and the measurement uncertainty, while the horizontal error bars are the RMS of the $\psi$ coordinate mapped from a pressure constrained EFIT [11] equilibrium.

Looking both at the $Z_{\text{eff}}$ evolution and at the neon fueling rate, it is clear that the increase in $Z_{\text{eff}}$ starts ~200 ms after neon is injected into the plasma, therefore it is reasonable to assume that the increase in $Z_{\text{eff}}$ is due to the neon seeding.

In these shots the deuterium source is provided by a D gas flow rate ($\Gamma_e(D) = 0.4 \times 10^{22}$ el s$^{-1}$) and by 2 mm D pacing pellets at $f = 45$ Hz, while the neon seeding rate in JPN 96994 is equal to $\Gamma_e(\text{Ne}) = 0.8 \times 10^{22}$ el s$^{-1}$. The amount of neon injected into the plasma is lower than the one injected in highly radiating scenarios [4, 13], where the operation is pushed towards detachment, while in the baseline plasmas analyzed here the divertor remains attached.

The motivation of this work comes from the experimental observation of the slightly higher energy confinement time (+14.0%) and neutron rate (+17.9%) of the Ne seeded shot with respect to the unseeded one, as we can see in the bottom box of figure 1. The percentage values are computed in the time interval [11.37–11.87 s] in order to avoid the presence of sawteeth. This increase in performance can be caused by a series of concatenated effects, often difficult to disentangle from each other given the high non-linearity of thermonuclear plasmas, which will be discussed in section 4.

What is important to underline is that the Ne seeded shot shows a lower electron density at the plasma edge and a higher ion temperature in the core, which are visible both from the experimental time traces of figure 1 and from the experimental profiles of figure 2. Looking at the electron density profile (box (a) of figure 2), we can see that the pedestal height is reduced from an average value of $5.2 \times 10^{19}$ m$^{-3}$ in JPN 96730, to

a value of $4.1 \times 10^{19}$ m$^{-3}$ in JPN 96994, whereas the values close to the magnetic axis remain very similar to each other. This lower density at the plasma edge can be beneficial for the performance, allowing for a deeper penetration of NBI heating.

For what concerns the ion temperature profile (box (c) of figure 2), the higher core ion temperature is probably due to the higher ion temperature in the pedestal region, that propagates into the core due to the stiffness of the profiles [14]. This leads to an ion temperature in the core of $T_i \approx 9.31$ keV in JPN 96994, with respect to $T_i \approx 8.4$ keV in JPN 96730. The higher ion temperature in the core is clearly beneficial for the performance of the Ne seeded shot.

In the bottom box of figure 2 we can see that the experimental profiles of the toroidal rotation are almost superimposed.

## 3. Modelling the discharges

The simulations presented in this study are performed with the JINTRAC suite of codes [7], using the first-principle transport model QuaLiKiz [8, 9], coupled to the 1.5-dimensional transport code JETTO [15]. JETTO is the code that solves the transport equations for the ion density, the ion and electron temperature and the main ion rotation. It is a 1.5-dimensional transport code that averages the transport equations on the magnetic flux surfaces computed by the equilibrium solver. It needs a transport model to describe the turbulent fluxes of heat and particles. QuaLiKiz is a quasilinear gyrokinetic code used to compute the turbulent transport from the magnetic axis up to the pedestal top. The simulations are performed in a fully predictive way, meaning that the evolution of the plasma current density, ion density, electron and ion temperature and plasma rotation, as well as the evolution of the impurity density, is predicted.

The impurity transport is computed with SANCO [16], which includes the neoclassical transport provided by NCLASS [17] and the anomalous transport from QuaLiKiz. The code is taking into account an impurity mix of Be, Ne, Ni and W, whose composition is obtained with a method described in [18], in agreement with the estimate from spectroscopy [19, 20]. In order to model the neon seeding in JPN 96994, the Ne particle source is adjusted in SANCO to match the experimental time trace of $Z_{eff}$, which increases from a value of 1.9–2.3 during the simulated time interval.

The initial conditions for the electron density and temperature profiles are taken from high resolution Thomson scattering measurements [21], while for the ion temperature and toroidal rotation profiles are taken from beam charge exchange spectroscopy [22].

The boundary conditions are imposed at the separatrix, which is considered to be the position where $T_e = T_i = 100$ eV.

The transport in the pedestal region is empirically modelled according to the following methodology (presented and validated in [23]). The heat transport in the edge transport barrier (ETB) is adjusted in order to match the experimental height of the temperature pedestal. The width of the pedestal is imposed to match the experimental value. Once the heat transport in the ETB has been fixed, we assumed a $\chi/D = 4$ in the pedestal and tuned the gas puff particle source in FRANTIC [24], by means of a feedback loop, to match the density at the top of the ETB. The thermal diffusivity $\chi$ and the particle diffusivity $D$ are assumed to be the same for electrons and ions in the ETB.

Gas puff, pellets and wall particle sources are modelled in the simulations as gas puffing since it does not introduce significant changes in the modelling [18].

The equilibrium is computed self-consistently with the evolution of the kinetic profiles and the current density profile using the ESCO equilibrium solver [25].

The heat sources are computed by the PENCIL [26] and PION [27] codes for the NBI and ICRH respectively, where the synergy is taken into account self-consistently in JINTRAC (see, for example, [28]).

Sawteeth presence is also included in the modelling, using the Kadomtsev reconnection model [29]. The crash times are determined experimentally and given as inputs to the model.

The summary of the simulation settings and codes used in the modelling is provided in table 1.

The results of the simulations in terms of profiles and time traces are shown in figures 3 and 4 for JPN 96994, and in figures 5 and 6 for JPN 96730. In the figures we are comparing the simulated and experimental profiles of the electron density, electron temperature and ion temperature, as well as the time traces of the neutron rate, $Z_{eff}$ and bulk radiated power.

It can be seen that there is a general good agreement between the simulation and the experiment, especially in the pedestal values, meaning not only that QuaLiKiz is able to capture the transport in the core, but also that the empirical modelling of the pedestal is valid. To evaluate the agreement between the experimental and simulated profiles of the reference simulations, a standard deviation figure of merit, described in [9, 30], is used:

$$\Delta = \sqrt{\int_0^\rho \mathrm{d}x (f_{\mathrm{sim}} - f_{\mathrm{exp}})^2} \Big/ \sqrt{\int_0^\rho \mathrm{d}x f_{\mathrm{exp}}^2}.$$

Where $f_{\mathrm{sim}}$ is the simulated quantity and $f_{\mathrm{exp}}$ is the average experimental quantity; this formula does not take into account the systematic kinetic profiles measurements error, nor any source of potential error in the modelling, the evaluation of which is beyond the scope of this paper. Since QuaLiKiz is used only in the core, the standard deviations are evaluated up to the pedestal top, and summarized in table 2. The errors in the simulated profiles of $n_e, T_e, T_i$ with respect to the experimental ones are lower than the uncertainty of the measurements, combined with the fluctuation of the experimental points in the simulated time interval, in accordance with the overall good agreement visible in figures 3 and 5. Albeit the TEM heat transport in QuaLiKiz has been improved

**Table 1.** Summary of the simulation settings used in the integrated modelling of JPN 96730 and JPN 96994.

| | $T_e$ $T_i$ $n_e$ $\Omega$ | $n_{Be}, n_{Ne}, n_{Ni}, n_W$ | $P_{rad}$ | $P_{nbi}$ | $P_{icrh}$ | Neutrals | Equilibrium |
|---|---|---|---|---|---|---|---|
| Core $\Psi_N = [0 \sim 0.93]$ | Neoclassical: NCLASS<br>Anomalous: QuaLiKiz + 10% Bohm | SANCO | Prescribed from bolometry | PENCIL | PION | FRANTIC | ESCO |
| Pedestal $\Psi_N = [0.93–1]$ | Empirically modelled | | | | | | |

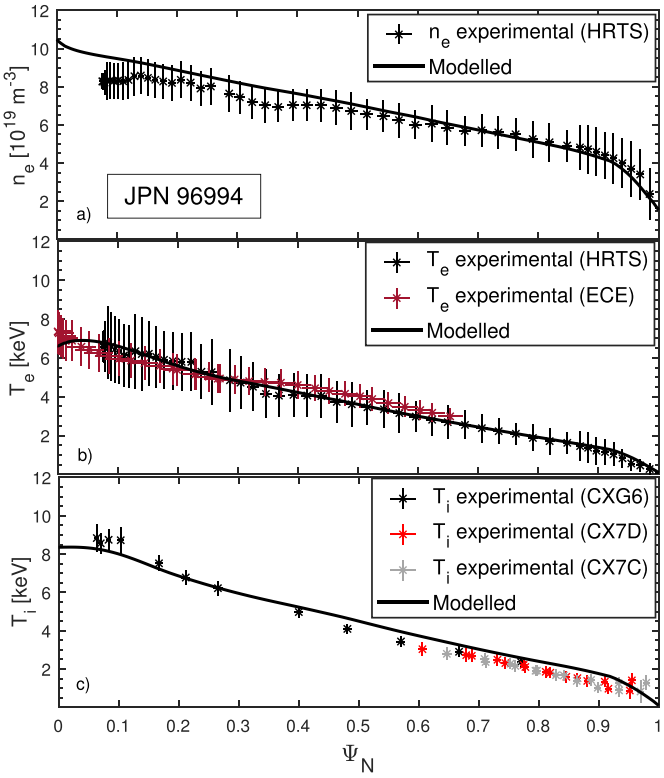


**Figure 3.** Comparison between experimental and simulated profiles of (*a*) electron density, (*b*) electron temperature and (*c*) ion temperature for JPN 96994 (Ne seeded). The experimental values are taken from HRTS measurements (electron density and temperature), electron cyclotron emission (electron temperature) and beam CX spectroscopy (ion temperature).

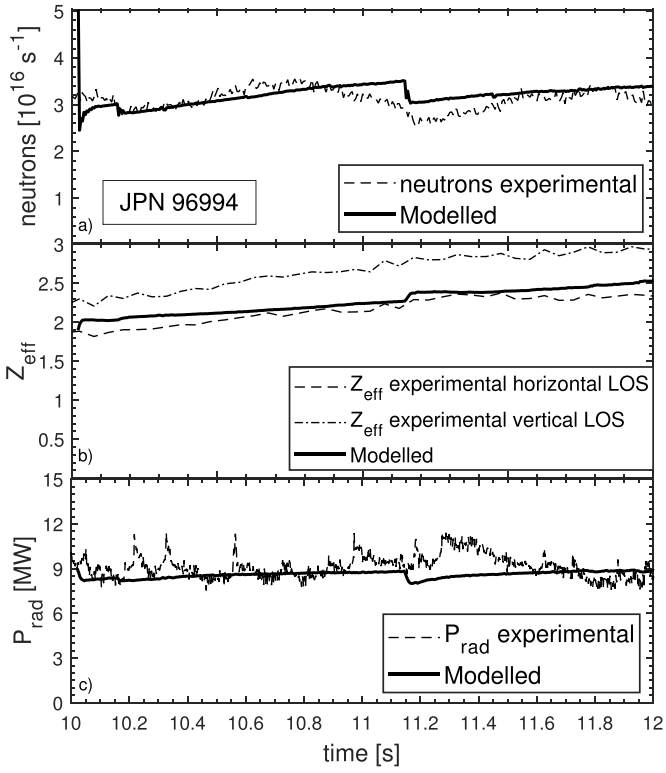


**Figure 4.** Comparison between experimental and simulated neutron rate (*a*), $Z_{eff}$ (*b*) and bulk radiated power (*c*) for JPN 96994. $Z_{eff}$ is inferred from Bremsstrahlung measurements along a vertical and a horizontal line of sight across the plasma and the bulk radiated power from bolometry.

by improving the collisionality operator [31], we can see from the density profiles that QuaLiKiz tends to overpredict the density peaking. Since it affects both simulations equally and only a small volume of the plasma ($\Psi_N < 0.2$), we consider the agreement suitable for our analysis.

For what concerns the rotation profiles, we found a standard deviation of 45% in JPN 96994 and of 60% in JPN 96730. In order to assess the sensitivity of the modelling results to the toroidal rotation profile, simulations with fixed experimental rotation profile were performed. In both shots, an increase in the electron and ion density peaking is found, which leads to a decrease in the core ion temperature, resulting in a decrease in the performance; the effect of the rotation profile on the neutron rate is therefore indirect. In figures 7 and 8 we can see the resulting kinetic profiles of the additional simulations performed. The increase of the density peaking and the decrease of the core ion temperature are visible in the green profiles of box (a) and (c) respectively, while the toroidal rotation is plotted in box (d). It seems not possible to match at the same time the toroidal rotation and the density in a fully predictive simulation of these particular baseline shots with QuaLiKiz.

However, imposing both the experimental profiles of the toroidal rotation and of the electron density allows to recover the temperature profiles and the performance in both shots (red profile). In fact, the difference in the neutron rate between the reference simulation and the one with interpretative rotation and density are of the order of 2–5%, which is lower than the RMS error of the model itself. Therefore, it seems that fixing the toroidal rotation profile is affecting the performance by increasing the density peaking and, consequently, decreasing the temperatures, but when the density is fixed, no difference in performance is found.

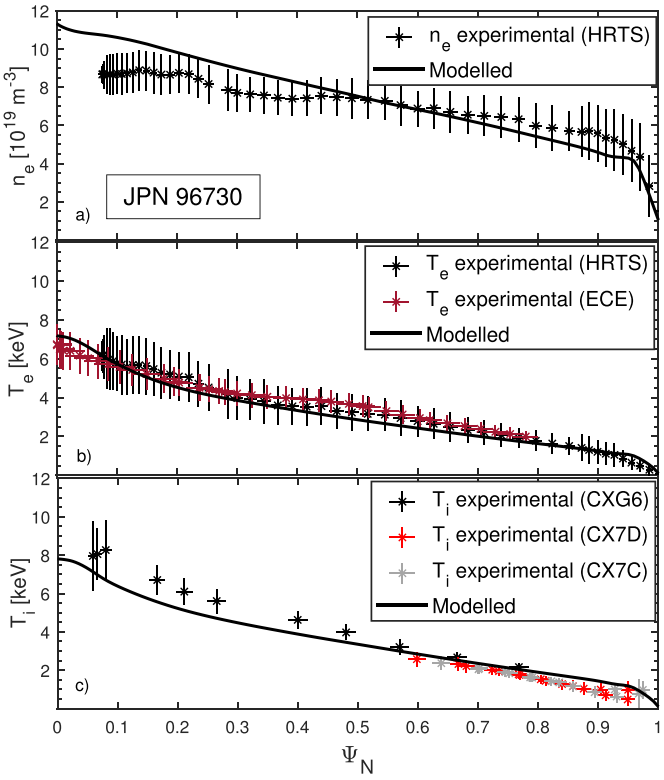


**Figure 5.** Comparison between experimental and simulated profiles of (*a*) electron density, (*b*) electron temperature and (*c*) ion temperature for JPN 96730 (unseeded). The experimental values are taken from HRTS measurements (electron density and temperature), electron cyclotron emission (electron temperature) and beam CX spectroscopy (ion temperature).

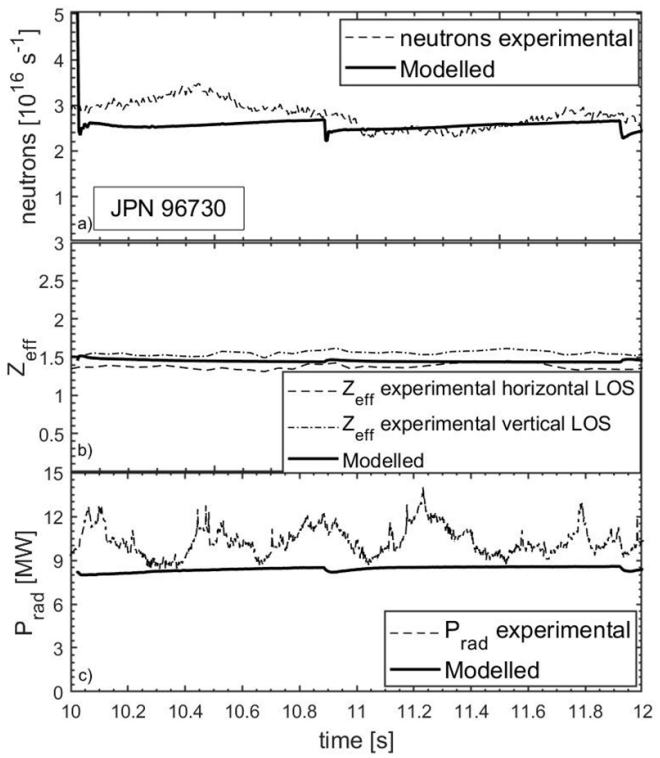


**Figure 6.** Comparison between experimental and simulated neutron rate (*a*), $Z_{\rm eff}$ (*b*) and bulk radiated power (*c*) for JPN 96730. $Z_{\rm eff}$ is inferred from Bremsstrahlung measurements along a vertical and a horizontal line of sight across the plasma and the bulk radiated power from bolometry.

## 4. Neon effects on transport

### *4.1. Transport and turbulence analysis*

After reproducing the profiles with QuaLiKiz, we investigate the difference in transport between the unseeded and Ne seeded pulses. Reaching a good agreement between experimental and simulated profiles and time traces is essential in order to allow the transport model to capture the physics of the experiment.

What emerges from the integrated modelling is that QuaLiKiz shows a reduction in the electron and ion thermal diffusivities of the Ne seeded shot with respect to the unseeded one, as we can see in figure 9, where the QuaLiKiz thermal diffusivities are plotted. The transport reduction is also visible in the reduction of the electron and ion heat fluxes (not shown here), which is stronger for ions than for electrons. The greatest reduction of $\chi$ comes from the anomalous contribution, suggesting the presence of a different level of turbulence in the two shots.

In order to understand the cause of the transport reduction, QuaLiKiz turbulence spectra are compared in figure 10. In the figure we plot the growth rates of the turbulence for JPN 96730 (left boxes) and JPN 96994 (right boxes), averaged in the time interval [11.37–11.87 s], in order to avoid the presence of sawteeth. In the upper boxes the growth rates are expressed in gyro/Bohm units, while in the lower boxes the growth rates are expressed in SI units and then normalized to $k_\theta^2$, resulting in a normalized growth rate with the dimension of a transport coefficient [m$^2$ s$^{-1}$]. The $x$-axis is the normalized toroidal flux $\rho$ and the $y$-axis is the product of the poloidal wavenumber $k_\theta$ and the main ion gyro radius $\rho_s$, defined as $\rho_s = \sqrt{T_{\rm e} m_{\rm i}}/q_{\rm e}B$, where $T_{\rm e}$ is the electron temperature, $m_{\rm i}$ is the ion mass, $q_{\rm e}$ is the electron charge and $B$ is the magnetic field. The gyro/Bohm normalized units are defined as follows:

$$\gamma_{\rm GB} = \gamma \sqrt{\frac{A_{\rm i,0} m_p}{T_{\rm e}}} a$$

where $\gamma$ is the growth rate expressed in SI, $A_{\rm i,0} m_p$ is approximating the main ion mass, $a$ is the minor radius and $T_{\rm e}$ is the electron temperature. For this microstability analysis, it is important to underline that the application of QuaLiKiz is restricted to the region up to the pedestal top and that its dispersion relation accounts for trapped and passing ions and electrons, i.e. it covers ion temperature gradient (ITG)-TEM and electron temperature gradient (ETG) ranges [8]. The ITG and ETG instabilities, whose scales range from $0 \lesssim k_\theta \rho_s \lesssim 1$ for ITG and $3 \lesssim k_\theta \rho_s \lesssim 30$ for ETG, are driven by gradients of the ion and electron temperature respectively.

As it can be seen from figure 10, going from the unseeded (left boxes) to the Ne seeded (right boxes) shot, we find a reduction in the growth rates of both ITG (low $k_\theta \rho_s$) and ETG

**Table 2.** Standard deviation figures of merit of JPN 96994 and JPN 96730 profiles of figures 3 and 5.

| Shot | Zone | $\Delta_{n_e}$ | $\Delta_{T_e}$ | $\Delta_{T_i}$ | $\Delta_{v_{tor}}$ |
|---|---|---|---|---|---|
| JPN 96994 | $\Psi_N = [0.05–0.93]$ | 8.0% | 3.9% | 8.1% | 44.7% |
| JPN 96730 | $\Psi_N = [0.05–0.95]$ | 12.6% | 8.9% | 15.1% | 60.0% |

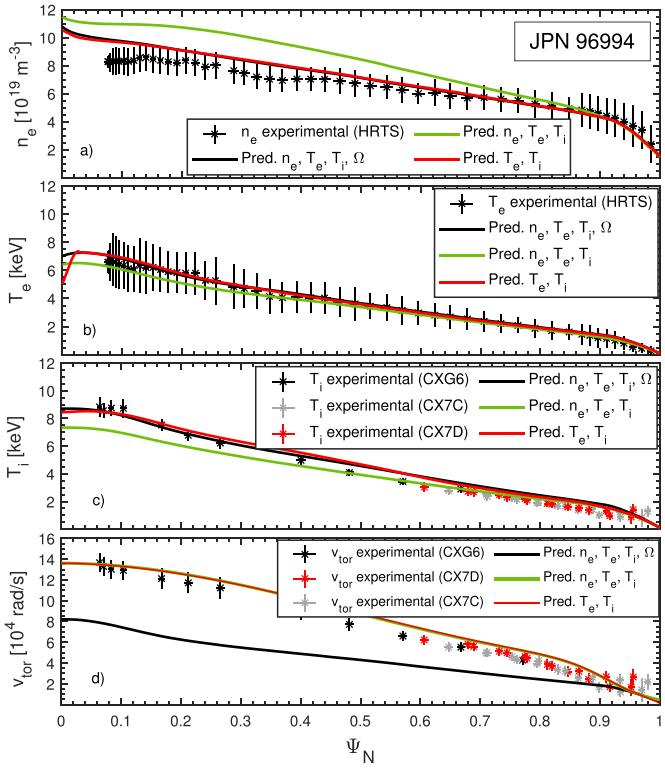


**Figure 7.** Profiles of the electron density (*a*), electron temperature (*b*), ion temperature (*c*) and toroidal rotation (*d*) for shot JPN 96994. The black solid line is the reference fully predictive simulation, in the green one we are predicting $n_e, T_e, T_i$ and in the red one we are predicting $T_e$ and $T_i$.

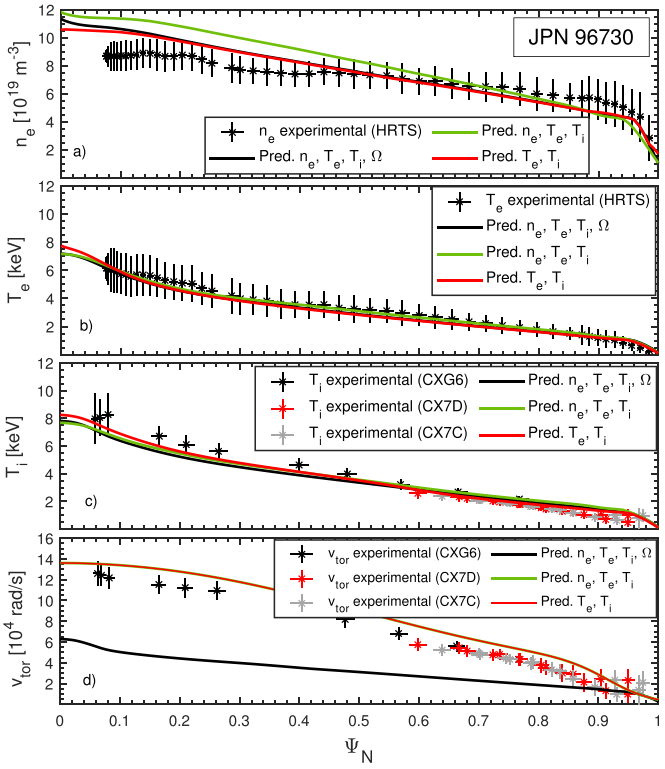


**Figure 8.** Profiles of the electron density (*a*), electron temperature (*b*), ion temperature (*c*) and toroidal rotation (*d*) for shot JPN 96730. The black solid line is the reference fully predictive simulation, in the green one we are predicting $n_e, T_e, T_i$ and in the red one we are predicting $T_e$ and $T_i$.

(high $k_\theta \rho_s$) modes. The decrease in the ETG modes is highlighted in the upper boxes of figure 10, while the decrease in the ITG modes is more clear in the lower boxes due to the normalization by $k_\theta^2$. This reduction seems to be stronger for ETG and, specifically, for $0.4 \lesssim \rho \lesssim 0.9$. For $\rho \lesssim 0.2$ the growth rates are zero and QuaLiKiz does not find any unstable mode; this reflects also on the QuaLiKiz contribution to the $\chi$ being zero in that region.

The turbulence stabilization can be caused by a series of non-linear effects which can be difficult to disentangle from each other. It has been argued in other papers that the ETG modes tend to be stabilized by higher $Z_{\text{eff}}$ [2, 3, 32] and higher $T_e/T_i$, while the ITG modes are stabilized by higher $Z_{\text{eff}}$ [33], higher $T_i/T_e$ [34, 35] and larger $\mathbf{E} \times \mathbf{B}$ shear [2, 3].

Impurity-induced reduction of ETG modes, together with ITG stabilization by $\mathbf{E} \times \mathbf{B}$ shear and high $T_i/T_e$, could be acting synergistically to reduce the transport and improve the global confinement in JPN 96994.

Similar results are obtained in highly radiating scenarios at JET [4, 5, 13], where the modelling identifies in the reduced core transport (via ITG and ETG turbulence stabilization) and in the increased pedestal $T_i$ and $T_e$ the causes for the improved performance with neon. However the baseline shots presented in this paper have lower neon seeding, lower recycling, lower gas puff, lower edge collisionality and a higher performance with respect to the ones presented in [4], in which the divertor is pushed towards detachment.

The effect of $\mathbf{E} \times \mathbf{B}$ shear, $T_i/T_e$ ratio and impurities on turbulence stabilization for JPN 96994 has also been studied in [36], using the GENE [37] gyrokinetic code at $\rho = 0.8$ and obtaining similar results.

### 4.2. Effects on performance

There are two main effects of neon seeding on transport: a direct effect on the turbulence stabilization and an indirect effect

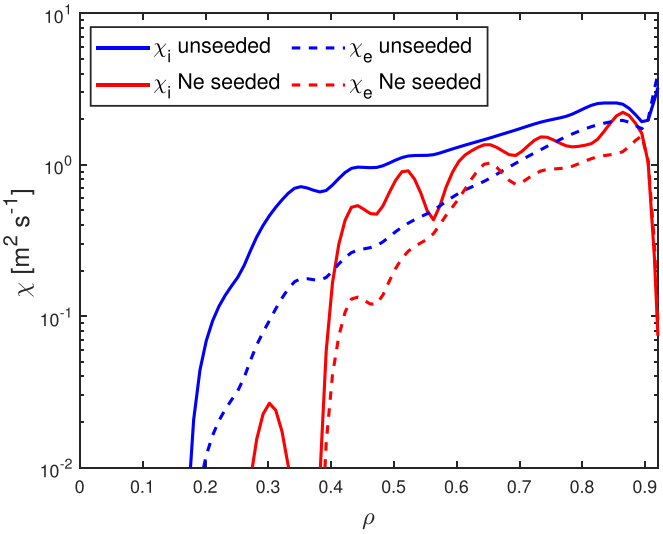


**Figure 9.** QuaLikiz electron (dashed line) and ion (solid line) thermal diffusivities for JPN 96994 (red) and JPN 96730 (blue), averaged between [11.37–11.87 s] and plotted in logarithmic scale against the normalized toroidal flux $\rho$, up to the top of the barrier position ($\rho_{\mathrm{TOB}} \sim 0.92$). From this comparison we can see the transport reduction of the Ne seeded shot captured by QuaLiKiz. The values for $\rho \gtrsim 0.92$ are imposed in the empirical modelling of the pedestal and are not computed by QuaLiKiz.

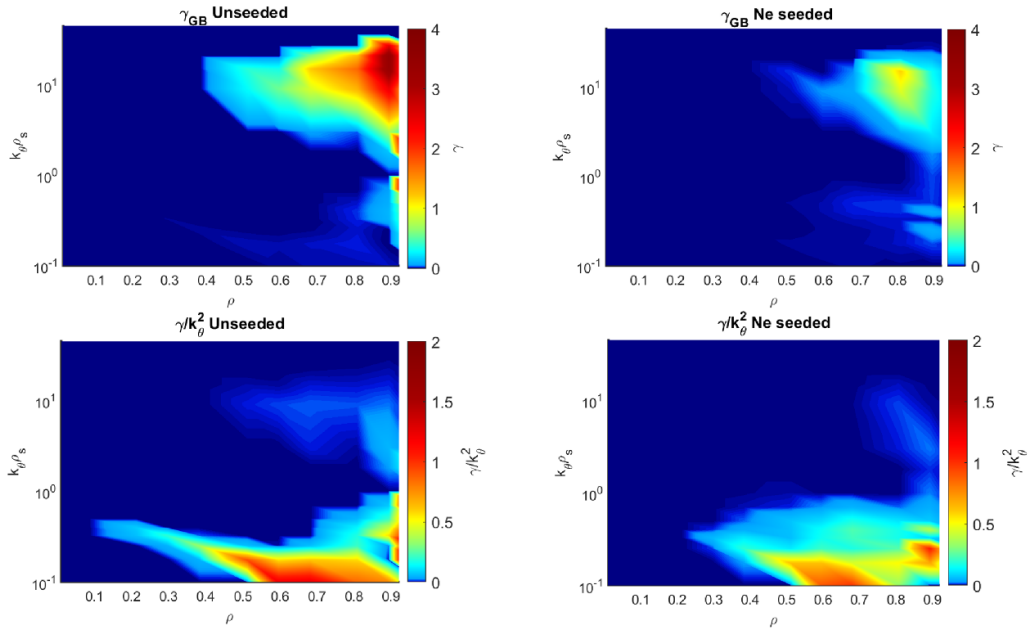


**Figure 10.** QuaLiKiz turbulence spectra for JET shot #96370 (left boxes) and JET shot #96994 (right boxes). The $x$-axis is the normalized toroidal flux $\rho$, the $y$-axis is the product of the poloidal wavenumber $k_\theta$ and the main ion gyroradius $\rho_s$, while the colormap represents the growth rate $\gamma$ of the turbulence. The growth rates are plotted both in gyro Bohm$^{-1}$ units (upper boxes) and in SI units normalized to $k_\theta^2$ (lower boxes) in order to highlight both the reduction of the ETG modes and of the ITG modes respectively. The $\gamma$ are averaged between 11.37 and 11.87 s, in order to avoid the impact of sawteeth.

on the pedestal parameters. Both of these effects are contributing to the higher performance in terms of neutron rate and confinement of the neon seeded shot.

In order to disentangle the effects of neon seeding, further modelling of JPN 96730 was carried out, which resulted in two additional simulations with the following characteristics:

- On the reference modelling of JPN 96730 we impose the same neon seeding used for reproducing JPN 96994;
- On the reference modelling of JPN 96730 we impose the same pedestal parameters used for reproducing JPN 96994.

The simulation settings, the initial conditions and the boundary conditions are the ones described in section 3. Since we are modelling the pedestal empirically, when we impose the pedestal parameters, we are actually imposing the same gas puff particle source and the same values of $\chi$ and $D$ used to match the $n_e$, $T_e$ and $T_i$ values at the top of the barrier.

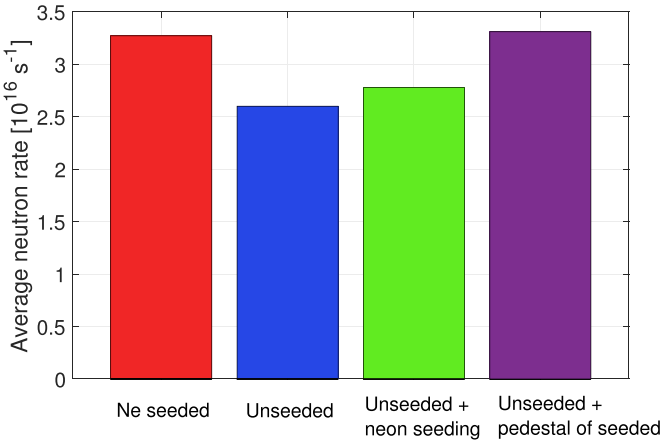


**Figure 11.** Modelled neutron rates, averaged between [11.37–11.87 s], of the reference Ne seeded shot (red), reference unseeded shot (blue), unseeded shot with neon seeding (green) and unseeded shot with the pedestal of the seeded one (purple). Including the same amount of neon of the seeded shot into the unseeded one allows to gain ~7% in terms of neutron rate, while imposing the pedestal characteristics of the seeded shot in the unseeded one allows for a ~27% gain in performance.

In figure 11, we are showing the results in terms of the neutron rates of the simulations. The red and blue bars are the neutron yields of the reference modelling of the Ne seeded and unseeded shots respectively. The green bar is the neutron rate of the simulation in which neon is injected into the reference unseeded shot, while the purple bar is the simulation in which the pedestal of the seeded shot is imposed in the unseeded simulation. In both of the last two simulations the modelling predicts an increase in the performance of the unseeded pulse in terms of neutron rate. This increase is of ~7% when neon is injected and of ~27% when the pedestal is changed, showing a greater impact of the pedestal with respect to neon seeding in improving the performance of the shot. However, experimentally it seems to be the neon seeding that allows the achievement of a lower electron density and a higher ion temperature in the pedestal, leading to an indirect impact on performance.

In addition to this, comparing the heat fluxes of these simulations to the reference unseeded shot modelling, we found that the electron heat flux $q_e$ is not modified when imposing the pedestal of the seeded shot, while it is reduced by ~20% when injecting neon into the plasma, meaning that neon seeding is indeed affecting the electron thermal transport channel (probably via ETG stabilization).

Overall, these results suggest that the improvement in the confinement and performance of the neon seeded shot is due to a combination of improved pedestal parameters and impurity-induced turbulence stabilization with neon. The direct effect of neon on performance is through the stabilization of turbulences, which leads to a higher confinement by reducing the heat transport. The indirect effect is via changes of the pedestal values that are leading to higher performance. The pedestal change obtained experimentally with neon seeding, i.e. lower $n_e$ and higher $T_i$, is playing a major role in the global performance improvement.

## 5. Conclusions

We have presented the JETTO-QuaLiKiz-SANCO fully predictive modelling of two JET high-performance baseline plasmas, a Ne seeded shot (JPN 96994) and an equivalent unseeded one (JPN 96730), in order to investigate the effects of neon seeding on transport and confinement. The reason behind this work is the experimental observation of a slightly higher neutron rate (+17.9%) and energy confinement time (+ 14.0%) of the neon seeded with respect to the unseeded one, while sharing the same plasma parameters and heating powers.

The simulations are in good agreement with the experimental measurements for both of the analyzed shots, therefore allowing QuaLiKiz to capture the difference in transport between the pulses.

QuaLiKiz shows a reduction in the core ion and electron thermal diffusivities of the neon seeded shot with respect to the unseeded ones. Comparing QuaLiKiz turbulence spectra, we found a stabilization of ITG and ETG modes, visible in the reduction of the growth rates of these particular modes. Impurity-induced reduction of ETG modes, together with ITG stabilization by $\mathbf{E} \times \mathbf{B}$ shear and high $T_i/T_e$, could be acting synergistically to reduce the transport and improve the global confinement in JPN 96994.

In order to disentangle the contribution from the improved pedestal parameters with neon and the one from reduced transport by impurity-induced turbulence stabilization, further modelling was carried out. The modelling suggests that the improved pedestal is playing a greater role in the performance improvement with respect to neon seeding. In fact, imposing the pedestal parameters of the neon seeded shot on the unseeded one leads to a gain in performance of ~27%, while injecting neon in the unseeded shot leads to a ~7% gain.

## Acknowledgments

This work has been carried out within the framework of the EUROfusion Consortium, funded by the European Union via the Euratom Research and Training Programme (Grant Agreement No. 101052200—EUROfusion). Views and opinions expressed are however those of the author(s) only and do not necessarily reflect those of the European Union or the European Commission. Neither the European Union nor the European Commission can be held responsible for them.

## ORCID iDs

S. Gabriellini https://orcid.org/0000-0001-9488-5193
L. Garzotti https://orcid.org/0000-0002-3796-9814
V.K. Zotta https://orcid.org/0000-0002-3518-5178
C. Bourdelle https://orcid.org/0000-0002-4096-8978
F.J. Casson https://orcid.org/0000-0001-5371-5876
J. Citrin https://orcid.org/0000-0001-8007-5501
G. Pucella https://orcid.org/0000-0002-9923-2770
D. van Eester https://orcid.org/0000-0002-4284-3992

## References


[1] Lawson J.D. 1957 *Proc. Phys. Soc.* B **70** 6
[2] Staebler G.M., Jackson G.L., West W.P., Allen S.L., Groebner R.J., Schaffer M.J. and Whyte D.G. 1999 *Phys. Rev. Lett.* **82** 1692
[3] McKee G.R. *et al* 2000 *Phys. Plasmas* **7** 1870
[4] Giroud C. *et al* 2021 High performance ITER-baseline discharges in deuterium with nitrogen and neon-seeding in the JET-ILW *Preprint: 2020 IAEA Fusion Energy Conf. (Nice, France (virtual event), 2021)* (available at: https://nucleus.iaea.org/sites/fusionportal/Shared%2520Documents/FEC%25202020/fec2020-preprints/preprint0977.pdf)
[5] Marin M., Citrin J., Giroud C., Bourdelle C., Camenen Y., Garzotti L., Ho A., Sertoli M. and Contributors J. 2023 *Nucl. Fusion* **63** 016019
[6] Moradi S., Bourdelle C., Tokar M.Z., Litaudon X., Imbeaux F., Corre Y., Monier-Garbet P., Kalupin D. and Weyssow B. 2011 *Plasma Phys. Control. Fusion* **54** 015004
[7] Romanelli M. *et al* 2014 *Plasma Fusion Res.* **9** 3403023
[8] Bourdelle C., Citrin J., Baiocchi B., Casati A., Cottier P., Garbet X. and Imbeaux F. 2016 *Plasma Phys. Control. Fusion* **58** 014036
[9] Citrin J. *et al* 2017 *Plasma Phys. Control. Fusion* **59** 124005
[10] Garzotti L. *et al* 2019 *Nucl. Fusion.* **59** 076037
[11] Szepesi G. *et al* 2021 Advanced equilibrium reconstruction for JET with EFIT++ *47th EPS Conf. on Controlled Fusion and Plasma Physics* (*Sitges, Spain, 21–25 June 2021*) (*P3.1037*) (available at: http://ocs.ciemat.es/EPS2021PAP/pdf/P3.1037.pdf)
[12] Mailloux J. *et al* 2022 *Nucl. Fusion* **62** 042026
[13] Glöggler S. *et al* 2019 *Nucl. Fusion* **59** 126031
[14] Garbet X. *et al* 2004 *Plasma Phys. Control. Fusion* **46** 1351
[15] Cenacchi G. and Taroni A. 1988 JETTO: a free-boundary plasma transport code *Rapporto ENEA RT/TIB/88/5*
[16] Lauro Taroni L. 1994 *Proc. 21st EPS Conf. Controlled Fusion and Plasma Physics ECA* (*Montpellier, France, 27 June–1 July 1994*) (*18B Part I*) p 102
[17] Houlberg W.A., Shaing K.C., Hirshman S.P. and Zarnstorff M.C. 1997 *Phys. Plasmas* **4** 3230
[18] Zotta V.K. *et al* 2022 Predictive modelling of D-T fuel mix control with gas puff and pellets for JET 3.5 MA baseline scenario *48th EPS Conf. on Plasma Physics* (*P2a.115*) (available at: http://ocs.ciemat.es/EPS2022PAP/pdf/P2a.115.pdf)
[19] Czarnecka A., Zastrow K.-D., Rzadkiewicz J., Coffey I.H., Lawson K.D. and O'Mullane M.G. 2011 *Plasma Phys. Control Fusion* **53** 035009
[20] Sertoli M., Carvalho P.J., Giroud C. and Menmuir S. 2019 *J. Plasma Phys.* **85** 905850504
[21] Pasqualotto R., Nielsen P., Gowers C., Beurskens M., Kempenaars M., Carlstrom T. and Johnson D. 2004 *Rev. Sci. Instrum.* **75** 3891
[22] Hawkes N.C., Delabie E., Menmuir S., Giroud C., Meigs A.G., Conway N.J., Biewer T.M. and Hillis D.L. 2018 *Rev. Sci. Instrum.* **89** 10D113
[23] Zotta V.K. *et al* 2022 *Nucl. Fusion* **62** 076024
[24] Tamor S. 1981 *J. Comput. Phys.* **40** 104
[25] Cenacchi G. and Rulli M. 1988 Upgrading of an equilibrium transport code for a multispecies free-boundary plasma *ENEA Report* RTI/TIB(88)5
[26] Challis C.D., Cordey J.G., Hamnén H., Stubberfield P.M., Christiansen J.P., Lazzaro E., Muir D.G., Stork D. and Thompson E. 1989 *Nucl. Fusion* **29** 563
[27] Eriksson L.-G., Hellsten T. and Willen U. 1993 *Nucl. Fusion* **33** 1037
[28] Gallart D. *et al* 2018 *Nucl. Fusion* **58** 106037
[29] Kadomtsev B.B. 1975 *Sov. J. Plasma Phys.* **1** 710–5
[30] ITER Physics Basis editors 1999 *Nucl. Fusion* **39** 2175
[31] Stephens C. 2021 Advances in quasilinear gyrokinetic modeling of turbulent transport *PhD Thesis* University of California
[32] Jenko F. and Dorland W. 2002 *Phys. Rev. Lett.* **89** 225001
[33] Dominguez R.R. and Rosenbluth M.N. 1989 *Nucl. Fusion* **29** 844
[34] Kim H.-T., Sips A.C.C., Romanelli M., Challis C.D., Rimini F., Garzotti L., Lerche E., Buchanan J., Yuan X. and Kaye S. 2018 *Nucl. Fusion* **58** 036020
[35] Romanelli M., Regnoli G. and Bourdelle C. 2007 *Phys. Plasmas* **14** 082305
[36] Garcia J. *et al* 2022 *Phys. Plasmas* **29** 032505
[37] Jenko F., Dorland W., Kotschenreuther M. and Rogers B.N. 2000 *Phys. Plasmas* **7** 1904